Modeling the Impact of Ocean Circulation on Chlorophyll Blooms Around South Georgia, Southern Ocean

R. P. Matano[1] , **V. Combes[1]**, **E. F. Young[2]**, and **M. P. Meredith[2]**

[1]College of Earth, Ocean and Atmos. Sc., Oregon State University, Corvallis, OR, USA, [2]British Antarctic Survey, Cambridge, UK

Abstract The northeast periphery of the Scotia Sea hosts one of the largest chlorophyll-a blooms of the Southern Ocean. This bloom peaks to the northwest of the island of South Georgia, extending eastward for hundreds of kilometers. Although the Southern Ocean has many islands of similar size, South Georgia is ecologically one of the most significant: It not only sustains one of the Southern Ocean's largest and most diverse ecosystems but also constitutes its single most important region for biological carbon sequestration. While the exceptional nature of South Georgia's blooms has been recognized widely, both the physical processes that contribute to their fertilization and the reasons why these blooms are larger than those of other similar regions (e.g., Kerguelen or Crozet Islands) are poorly understood. We use the results of a high-resolution ocean model to investigate the physical processes that mediate the entrainment of deep, iron-rich waters into the surface layers of the South Georgia region. We show that the Southern Antarctic Circumpolar Current Front, the southernmost jet of the Antarctic Circumpolar Current (ACC), pumps iron-enriched waters from the deep ocean onto the bottom layers of South Georgia's shelf. These waters are upwelled along the northern coast of the island and are then exported into the Georgia Basin, where topographically steered circulation shields them from the dispersive effects of local currents and eddies, thus allowing the bloom development.

Plain Language Summary The growth of phytoplankton in the ocean is the base of the marine food web and is fueled by the supply of nutrients. In the Southern Ocean, this growth is anomalously strong downstream of islands and seamounts and very markedly so downstream of the island of South Georgia. We use a high-resolution ocean model to explain how the ocean circulation supplies nutrients to the South Georgia bloom and find that the pumping of iron-rich waters from depth onto the South Georgia shelf is key, as is upwelling of water on the northern side of the island and subsequent flow into the open ocean beyond. This marine growth supports a rich and diverse ecosystem, including some species which are commercially valuable.

1. Introduction

South Georgia (SG; 54.5°S, 37°W) is a mountainous island located in the northeast corner of the Scotia Sea in the Southern Ocean (Figure 1a). It sits on a relatively deep and rugged shelf, which extends from 50 to 150 km from the coast before dropping steeply into the deep ocean. SG shelf waters are surrounded by the turbulent flow of the southern branch of the Antarctic Circumpolar Current (ACC), termed the Southern ACC Front (SACCF), and lie under the persistent influence of strong westerly winds. Reports from the early discovery investigations hypothesized that the physical properties of SG's waters reflect influences from the Scotia and the Weddell Seas (Clowes, 1938; Hardy & Gunther, 1935; Hart, 1934). Later studies have shown that these waters are associated with the SACCF, which wraps around the southern limit of the SG shelf before bifurcating into a branch flowing toward the west and another toward the northeast (Korb & Whitehouse, 2004; Meredith, 2003; Orsi et al., 1995; Thorpe et al., 2002; Figure 1a). Comparatively little is known about the details of the SG shelf circulation, particularly in the southern portion of the island (Ward et al., 2007), although ship sections and drifter deployments have provided information off the northern and northwestern coasts (Korb & Whitehouse, 2004; Meredith, 2003), and previous modeling studies have described the broad features of variability in the shelf circulation (Young et al., 2011, 2014). Hydrographic observations indicate that shelf waters can be fresher and warmer than those farther offshore as a result of water mass retention, freshwater discharges, solar heating, and mixing (Whitehouse et al., 1996). Temporal variability in each of these processes can lead to marked difference in onshelf/offshelf gradients
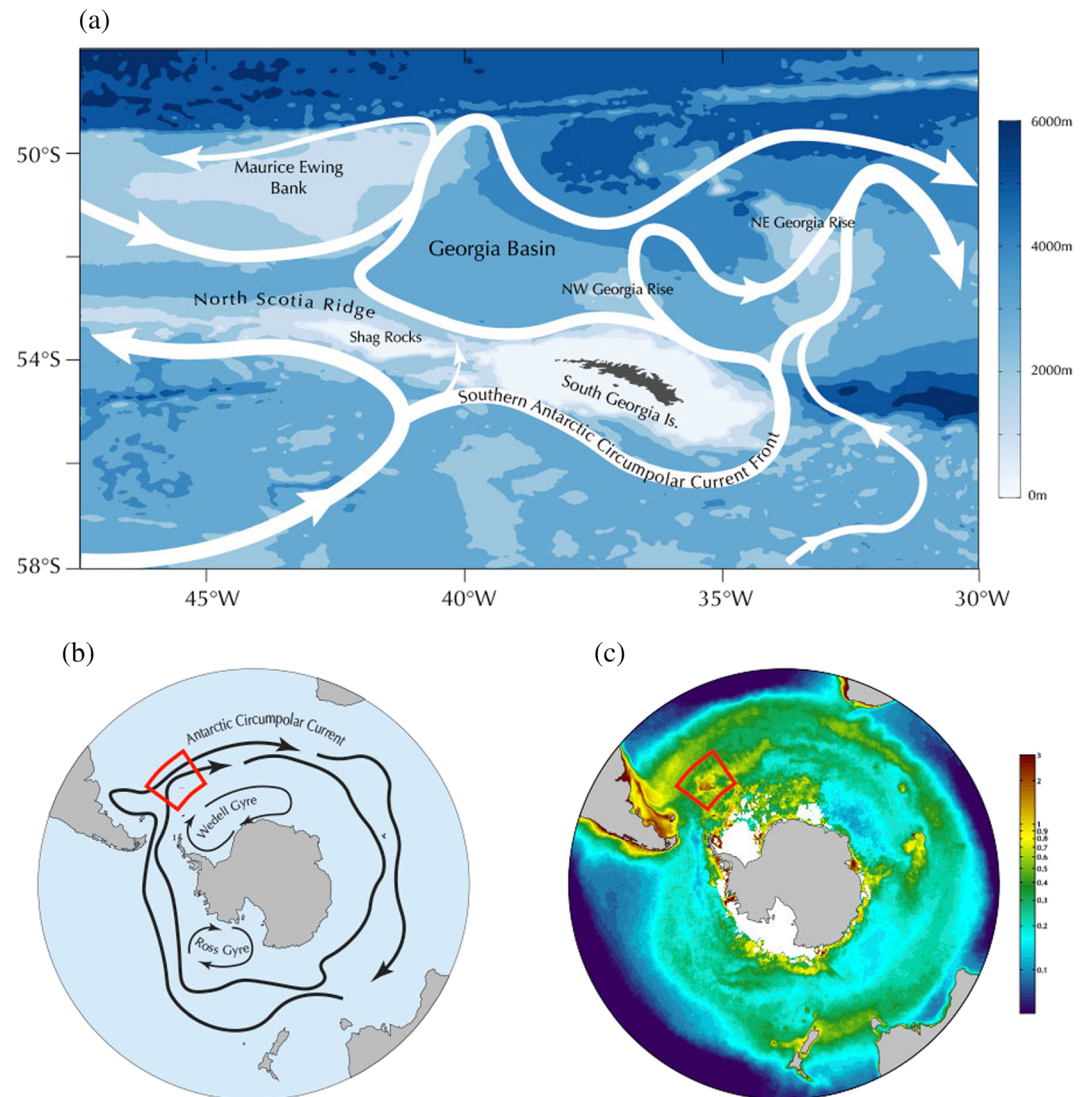
Figure 1. South Georgia (SG) circulation: (a) schematic representation of the time averaged circulation in the upper layer of the ocean, (0–500 m). This schematic is based on the model results and is in agreement with the patterns inferred from ARGOS floats and from satellite altimetry data. Background colors represent the bottom topography of the region; (b) schematic of the large scale circulation in the Southern Ocean, red lines mark the location of the SG region; (c) SeaWIFS climatological (1998–2010) December distribution of chlorophyll-a (mg/m^3).

(Meredith et al., 2005). On occasion, the thermohaline differences between shelf and off-shelf waters lead to the formation of a geostrophically balanced shelf break front (Brandon et al., 1999). Likewise, little is known about the influence of the deep ocean circulation over the SG shelf, although it has been observed that eddies and meanders of the SACCF might have a strong influence on the SG ecosystem (Trathan et al., 2003).

In contrast to the high-nutrient, low-chlorophyll conditions that prevail in most of the Southern Ocean (SO), SG is a highly productive region with a thriving marine ecosystem characterized by large colonies of higher predators such as fur seals, albatrosses, penguins, and whales (Atkinson, 2001). This island hosts some of the largest chlorophyll-a blooms in the SO (Figure 1c). They peak in the northwest portion of the shelf and extend eastward for hundreds of kilometers (Robinson et al., 2016; Venables & Meredith, 2009; Figure 2a). The Georgia Basin, which lies in the wake of SG's plume, is particularly productive, with chlorophyll blooms of up to 20 mg/m^3 and mean values larger than 3 mg/m^3 (Korb & Whitehouse, 2004). These blooms can be sustained for several months and support an immensely rich food web, and some components
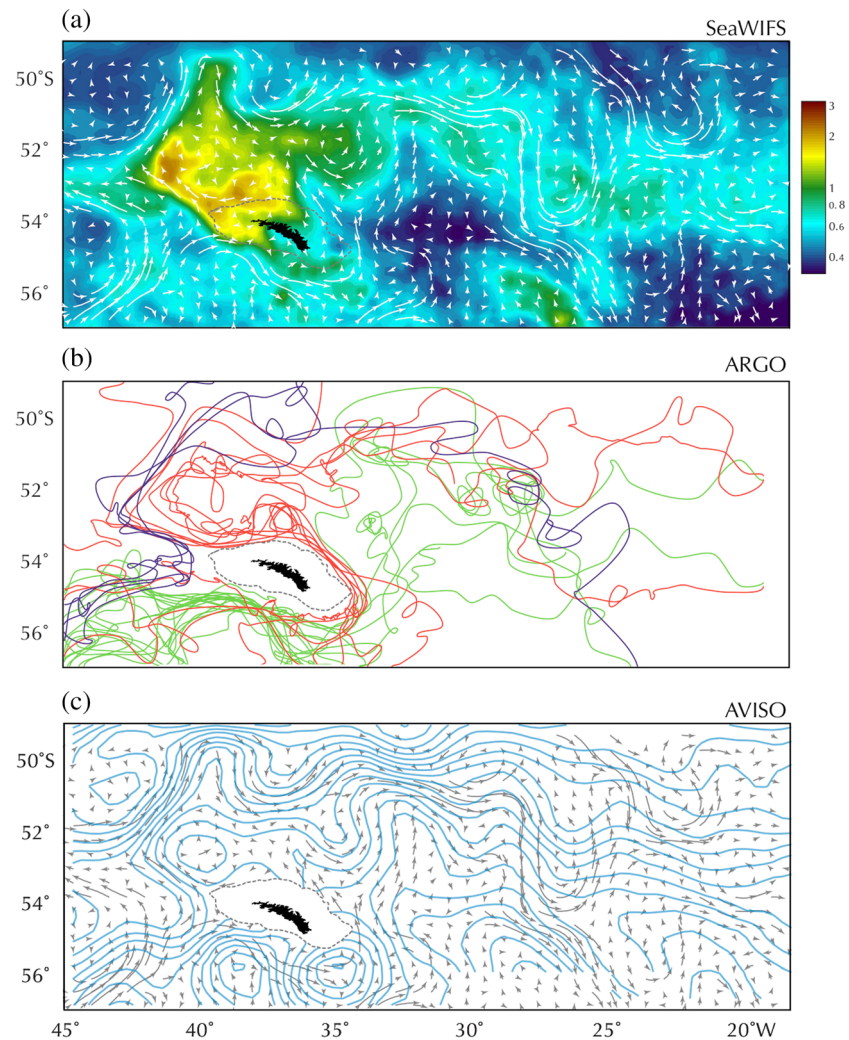
Figure 2. Model and observations: (a) summer mean chlorophyll-a distribution (color) from SeaWiFS (mg/m^3) and time mean model velocities (vectors); (b) ARGO floats trajectories. Contour colors highlight the three dominant pathways of the SACCF in the region. The dotted line surrounding SG marks the 500 m isobath; (c) mean dynamic height from AVISO altimetry data (light blue contours) and model velocities (vectors).

of which constitute a valuable commercial resource (Atkinson, 2001; Korb & Whitehouse, 2004). Although SG′s blooms are deemed to be the strongest biological carbon sink in the Southern Ocean (Schlitzer, 2002), their uniqueness, in terms of their magnitude and extent, has not been fully explained. Enhancement of productivity and biomass has been reported to occur in the wake of other Southern Ocean islands (e.g., Heywood et al., 1990; Palacios, 2002; Signorini et al., 1999). At SG, these enhancements are thought to be sustained by the entrainment of iron and other micronutrients from benthic or glacial sources (Borrione et al., 2014; Holeton et al., 2005; Korb & Whitehouse, 2004; Whitehouse et al., 1999). de Baar et al. (1995) documented the relationship between elevated concentrations of chlorophyll-a and iron in a section along 6°W, ascribing the elevated iron levels (up to 4 nmol m^{-3}) to an upstream sediment source, most likely SG. SeaWiFs data show that the elevated chl-a levels documented by de Baar et al. (1995) are frequently part of a continuous feature extending from the SG shelf. It is difficult to ascertain the sustenance of SG blooms (Robinson et al., 2016). Large blooms of other islands (e.g., Crozet and Kerguelen) have been observed, but they lack the exceptional magnitudes and extents observed in the SG region (Korb & Whitehouse, 2004).
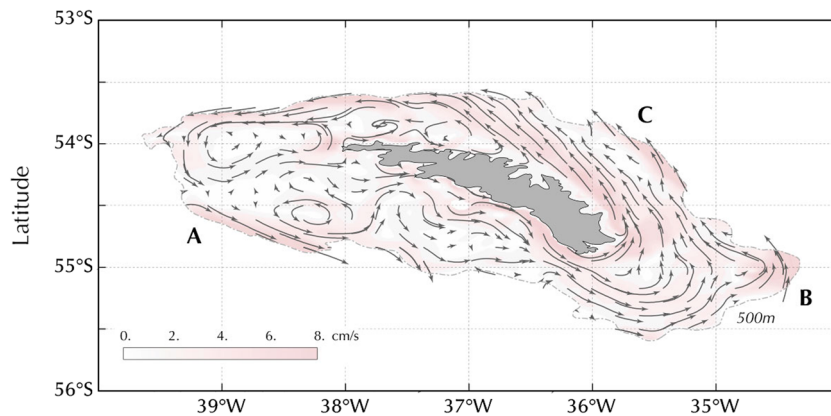
Figure 3. SG shelf circulation: Time mean, depth-averaged circulation over the SG shelf ($h < 500$ m) produced by the experiment CTRL. Vectors lengths and colors are proportional to speeds.

Description of the physical characteristics of the waters around SG began with the early discovery investigations (Deacon, 1933; Harmer, 1931). However, incomplete understanding of the physical mechanisms sustaining the extraordinary productivity of SG remains a consequence of the remoteness of the region and the harsh climate making it extremely difficult to collect in situ information. Most of the information about the local circulation has been inferred from hydrographic expeditions, with emphasis on the northern portion of the island (Korb & Whitehouse, 2004; Thorpe et al., 2002), and a small number of drifter releases (Korb & Whitehouse, 2004; Meredith, 2003). Numerical modeling offers an alternative approach but requires resolution of the small-scale physical processes that control exchanges between SG and the open ocean, for example, Young et al. (2011) and Young et al. (2014).

In this article, we investigate the physical processes underlying SG's high primary productivity. Using the results of a suite of high-resolution ocean model simulations, we characterize the SG shelf circulation and its interactions with the open ocean. In what follows, the term *shelf* designates the oceanic region with depths smaller than 500 m, *open-ocean* the contiguous oceanic realm, and *deep-ocean* the portion of the water column below the upper mixed-layer.

2. Model Description

The model used in this study is the nested Adaptive Grid Refinement in Fortran (AGRIF) version of the Regional Ocean Modeling System (ROMS; Debreu et al., 2011; Shchepetkin & McWilliams, 2005). The model is configured with an eddy-permitting parent grid within which there are embedded two child grids of increasingly higher horizontal resolution (Figure S1 in the supporting information). The parent grid extends 360° in the longitudinal direction and from Antarctica to 15.2°N. It has a spatial resolution of 1/4° and 40 terrain-following levels in the vertical. The first nested child grid encompasses the Scotia Sea and has a spatial resolution of 1/12° with similar vertical resolution. This two-way nested configuration is initialized using January 1, 1994, Hybrid Coordinate Model (HYCOM) data. At the northern boundary, the model is forced by the HYCOM climatological data. At the surface, the model is forced by monthly averaged ERA-Interim wind stress (Dee et al., 2011) for the period 1995–2016 and monthly climatology COADS heat and freshwater fluxes (Da Silva et al., 1994). These fluxes are corrected by including a tendency restoring term to the HYCOM sea surface temperature/salinity (SST/SSS) climatology. The second child grid encompasses the region around SG and has a horizontal resolution of 1/36° (~2 km) and 40 vertical levels. The model uses data from the General Bathymetry Charts of the Ocean (GEBCO) updated with echo sounder data collected by the British Antarctic Survey (Young et al., 2011). This model configuration, which will henceforth be called CTRL, represents the benchmark against which additional process-oriented experiments (described in subsequent sections) will be compared. Tidal forcing is represented by the first eight tidal components of the tide-generating potential to the surface pressure gradient of the model. Horizontal mixing is represented with a biharmonic operator, vertical mixing with a K-Profile Parameterization scheme (Large et al., 1994) and bottom friction with a quadratic formulation. The CTRL experiment was initialized

with temperature and salinity fields interpolated from a spin-up performed with the parent/first child nested model configuration and forced at the surface with monthly climatological momentum, heat, and freshwater fluxes from the same experiment. Further description of the parent model spin-up and comparison with observations can be found in Combes and Matano (2014, 2019) and Matano et al. (2019). CTRL was integrated over a 5-year period. The last 3 years of this integration are used in the analyses presented here.

3. SG Circulation

3.1. Open Ocean Circulation

The flow of the ACC in this locality generates three distinct circulation patterns around SG (Figure 2b). A portion of this current flows through the deep gap immediately west of the SG shelf (blue trajectories, Figure 2b), while the other rounds the southern slope of the shelf before bifurcating into a branch flowing toward the Georgia Basin (red, Figure 2b), and the other continuing its northeastward course (light green, Figure 2b). Model results compare well with observations (Figure 2). Comparison with Argo float trajectories, for example, shows that the model captures the mean flow structure and the overall characteristics of individual trajectories (Figures 2a and 2b). Model results are also in good agreement with AVISO dynamic mean topography (Figure 2c). These agreements—noteworthy because model and observations do not represent the same time period—reflect the influence of the bottom topography on the ocean circulation. CTRL results are also consistent with circulation descriptions based on hydrographic observations (Meredith et al., 2005), drifter data (Korb & Whitehouse, 2004; Meredith, 2003), numerical simulations (Fach & Klinck, 2006; Matano et al., 2002; Thorpe et al., 2002; Young et al., 2011), and satellite data (Figures 2a and 2c).

3.2. Shelf Circulation

CTRL shelf circulation is rich in small-scale structures shaped by its rugged bottom topography (Figure 3). The transit of the SACCF around the shelf edge generates intrusions of open-ocean waters from the south and extrusions of shelf waters to the north. Along the southern coast of the island, there is a strong coastal current that, after rounding its eastern corner, flows across the shelf toward the open ocean. Shallow banks generate anticyclonic recirculation cells that dominate the circulation in the shelf's interior. Maximum mean speeds are observed near the coast (~8 cm/s), decreasing toward the shelf interior (2–4 cm/s). One of the most important features of this simulation is the development of an upwelling jet flowing eastward along the northwest coast of the island. As we shall show, this jet plays an important role in the uplifting of benthic and deep shelf waters toward the surface, and hence, it is an important contributor to the fertilization of the shelf waters. There are, however, no prior descriptions of this jet, most likely because none of the surveys conducted in this region operated sufficiently close to the coast to detect it. Its existence, however, is consistent with the high iron concentrations reported in this region (Borrione et al., 2014) and the local wind conditions.

3.3. Volume Transports

Alongshelf transports were computed in closely spaced transects extending between the coast and 500 m (Figure 4a). By mass conservation, the transport difference between any two transects represents the net exchange between the shelf and the open ocean, subject to surface fluxes and land runoff being minimal. Thus, increments of the alongshelf transport reflect onshore advection and decrements reflect offshore advection. Alongshelf transports are characterized by a minimum of 0.06 Sv (1 Sv $= 10^6$ m^3/s) at the western end of the shelf and a maximum of 0.75 Sv at the eastern end (Figure 4a). These order-of-magnitude variations reflect the vigorous exchanges between the shelf and the open ocean, which are represented by the slopes of the curves: positive slopes correspond with on-shelf flows (blue line) and negative slopes with off-shelf flows (orange line; Figure 4a). The strongest exchanges are observed at the eastern and western limits of the shelf and in the southwestern sector (Figure 4b). Peaks in the alongshelf transport curve are associated with locations where the SACCF is steered toward/away from the shelf. The first peak (Pt0 and Pt100), for example, marks the region where the SACCF first impinges on the shelf. The second peak (~Pt300) is at the easternmost end of the island, where the SACCF is forced against the shelf by the abrupt change of the shelf break orientation. This is also where the SACCF bifurcates. Note that at these points entrainments and detrainments are nearly compensating; thus, the net cross-shelf exchange in these regions is relatively small.
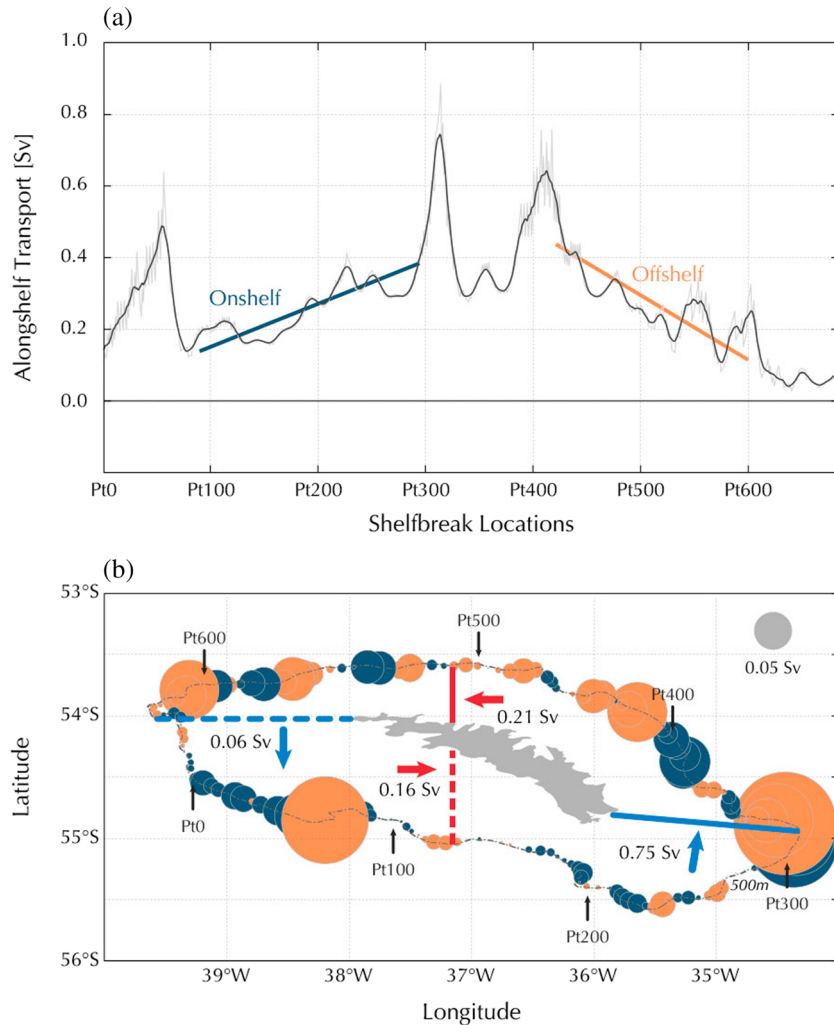
Figure 4. Transports in CTRL experiment: (a) Alongshelf transports between 500 m and the coast. Alongshelf locations are plotted in the horizontal axis. The slope of the curve represents the cross-shelf transports, positive values (blue) correspond with onshelf transport and negative (orange) offshelf; (b) orange and blue circles represent the magnitude and location of cross-shelf transports. Diameters are proportional to the magnitude and color to the direction (blue on-shelf and red off-shelf).

The amplitude of shelf/open-ocean exchange, which is represented by the difference between maximum and minimum in the alongshelf transport curve (Figure 4a), is ~0.7 Sv.

3.4. Obduction

SG′s exceptional blooms underline the importance of the physical processes contributing to the fertilization of its waters, in particular, to the entrainment of nutrient rich, deep, and benthic waters into the upper layers of the shelf. These entrainments, which are not driven by any single dynamical mechanism (i.e., upwelling or mixing), will be collectively referred to as *obduction*. To clarify the obduction processes, we injected two passive tracers, one in the slope (TRC_SLP) and the other over the shelf (TRC_SLF). The time evolution of the passive tracers is calculated with an advection/diffusion equation similar to that used for temperature and salinity (Marchesiello et al., 2009); advection is calculated with a third-order upstream scheme, horizontal diffusion with a bi-harmonic operator satisfying the Peclet constraint and vertical diffusion with a KPP parameterization (Large et al., 1994). Tracer TRC_SLP tags the obduction of deep and benthic waters of the open ocean; it is injected below 500 m where depths lie between 500 and 1,000 m with a release value of 1 (Figure S2). TRC_SLF tags the obduction of shelf benthic waters, and it is injected as a constant flux
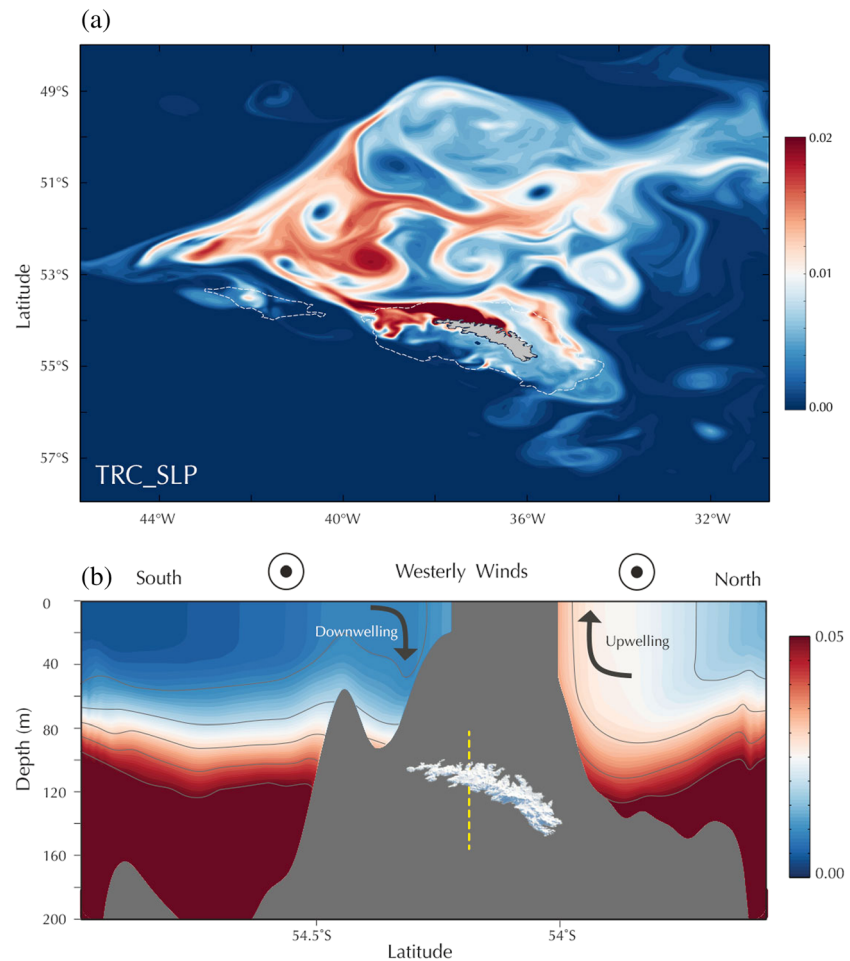
Figure 5. TRC_SLP: (a) snapshot of the surface tracer distribution after a 5-year diagnostic. TRC_SLP is injected along the continental slope and below 500 m depth; (b) vertical cross-section of TRC_SLP time mean concentration showing upwelling at the northern portion of the island and downwelling at southern. The yellow dotted line in the inset marks the location of the cross-section.

of 1/day in the bottom layer of the shelf. Both of these tracers are continuously released during a 5-year diagnostic integration, and their evolution is controlled by an advection/diffusion equation similar to that used for temperature and salinity.

Movie S1 shows the time evolution of TRC_SLP in the surface layer. It begins with the development of eddy-driven tracer pools along the shelf break and ends with a plume that closely resembles the chlorophyll satellite images (Figure 5a cf. Figure 2a). Most of the tracer obducted at the slope does not reach the surface, but it moves toward the SG coast in the intermediate and bottom layers of the shelf. After reaching the northwestern region, the tracer is brought to the surface by upwelling-favorable winds; whereupon, it is transported toward the open ocean. At the final stages of the diagnostic study, TRC_SLP forms a plume that peaks at SG's northern coast and extends into the Georgia Basin (Figure 5a). There, the topographic effects of the Maurice Ewing Bank and the North Scotia Ridge (Figure 1a) on the eastward flow of the ACC facilitate the steering and retention of the tracer, a phenomenon that—in the real ocean—is key to the local development of chlorophyll blooms.

The spatial structure of the tracer over the shelf is very complex. Snapshots show a close correspondence between tracer peaks and circulation vortices. Due to the weak density stratification, local seamounts generate Taylor caps, which can act as fluid trapping regions (Meredith, 2003). Particularly interesting is the development of a tracer maximum over the Shag Rocks shelf (Figure 5a), where the tracer was advected
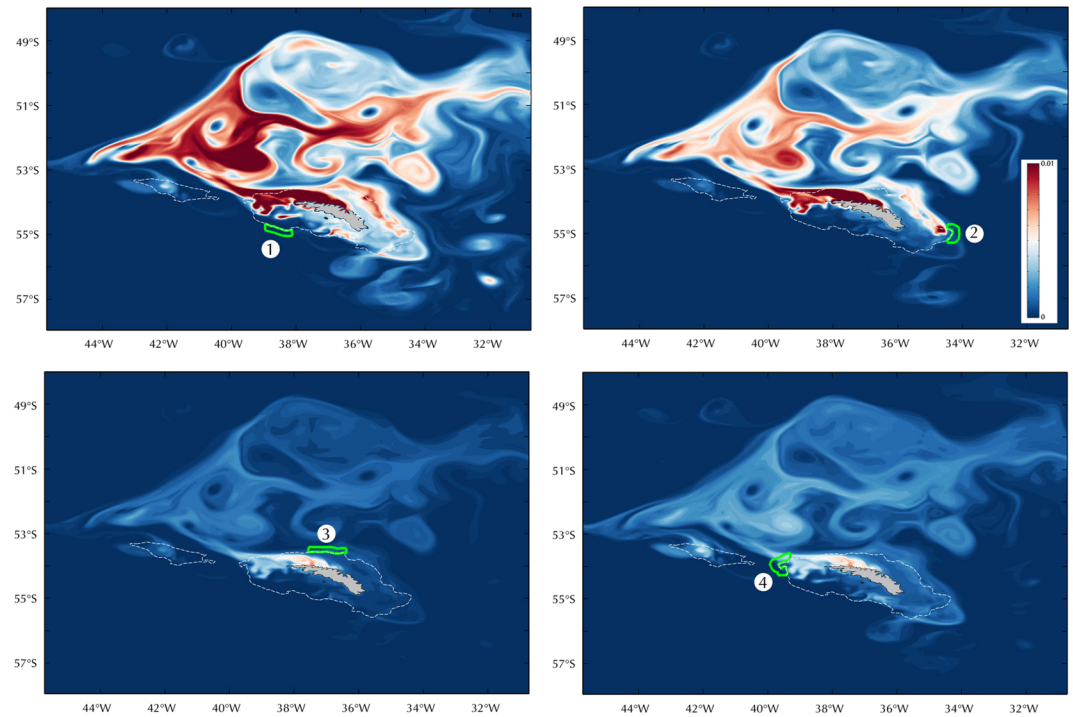
Figure 6. Obduction sites: Snapshots of the surface tracer distribution of tracers released at four different locations along the shelf slope. The green line shows each of the release sites. These tracers are injected below 500 m depth and the snapshot is taken at year five. The color bar of this figure is different than that of Figure 4 to allow a better visualization of the regions with relatively weak obduction.

by the westward branch of the SACCF and obducted and then trapped in the surface layer by a shelf-edge recirculation cell.

Whitehouse et al. (2008) observed that the northern portion of SG's shelf is biologically more productive than the southern portion. Our model results suggest that this disparity could be associated with circulation patterns. A latitudinal cross-section of TRC_SLP, for example, shows that while tracer-enriched waters from deeper and potentially more nutrient-replete levels reach the surface in the northern portion of the shelf, they remain confined to the deep layers in the south (Figure 5b). Westerly winds generate upwelling along the northern coast, bringing the tracer to the surface, and downwelling along the southern coast where obduction is prevented. The southern shelf, nevertheless, is not a biological desert. On occasion, it develops significant blooms (Whitehouse et al., 2008): These episodic blooms are consistent with the results of the numerical simulation, which show intermittent intrusions of iron-enriched waters driven by the transit of slope eddies or by the occasional advection of waters from the northern shelf (Movie S1). These transient iron-enriched flows are rapidly advected to the north and detrained into the deep ocean.

To identify the preferential sites for the obduction of TRC_SLP, we released passive tracers in selected areas around the shelf's slope (Figure 6). These tracers were injected below 500 m between the 500 and 1,000 m isobaths and were allowed to evolve over a 5-year period. At the end of this time, it is observed that the plumes from the southwestern and easternmost regions (sites 1 and 2, Figure 6) have higher tracer concentrations at the surface to the north of SG. All tracers show a maximum along the northern coast of SG, thus indicating that coastal upwelling is the preferential mechanism for the upper ocean entrainment of slope waters. Note that even the tracer from site 3, which is in a region dominated by the outflow of surface water, is entrained onto the shelf. This tracer is brought to the coastal upwelling region by the bottom layer circulation. Tracer released at site 4, the westernmost tip of the shelf, reaches maximum concentrations both at a nearby recirculation cell and over the Shag Rocks.

The time evolution of TRC_SLF is similar to that of TRC_SLP. After injection, it is transported to the northwestern upwelling region where it surfaces and is transported to the open ocean. The open ocean structure of
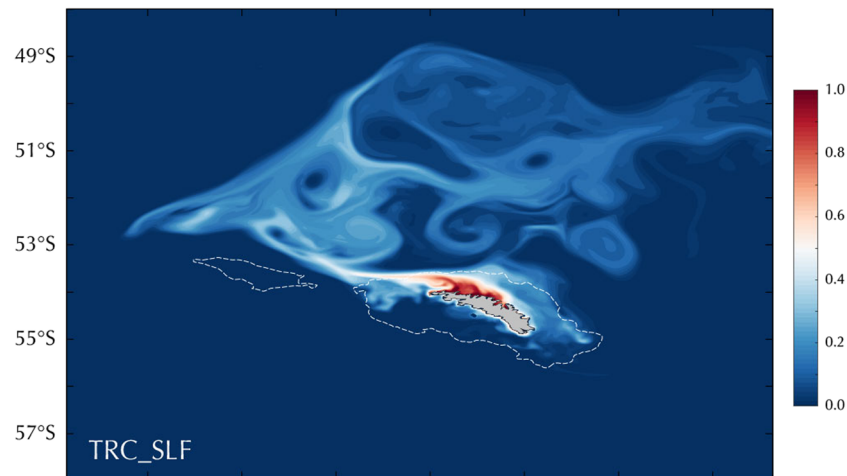
Figure 7. TRC_SLF: Snapshots of the surface tracer distribution after a 5-year diagnostic run with CTRL. TRC_SLF, specified as a constant flux in the bottom layer of the shelf. Note that the range of the color bar has changed.

the TRC_SLF plume is qualitatively similar to that of TRC_SLP (Figure 7). Over the shelf, however, TRC_SLF is largely constrained to the northwestern upwelling region. The common trait of both tracers is the maximum concentration in the northwestern portion of the shelf, which, once again, highlights the contribution of this upwelling system to the obduction of benthic waters. Note that quantitative differences between the two tracer concentrations do not reflect their relative weights but their different ages. Young et al. (2011) conducted a similar tracer release experiment, albeit for a shorter time period and a smaller geographical domain. The spatial structure of their plume, nevertheless, is similar to the one depicted here. The most important difference is that Young et al. (2011) did not find the high tracer concentration in the northwestern upwelling region because they released tracer over the entire water column.

3.5. Glacial Discharges

Besides the obduction of iron-rich waters, SG′s waters are also fertilized by the seasonal discharge of glacial melt. Young et al. (2011) developed an estimate of the magnitude and timing of the discharges of 51 glaciers (Figure 8a). Glacial discharges vary between 2 and 45 m^3/s with a maximum combined output of 1,200 m^3/s, peaking during the middle of summer (February) and dwindling toward the winter. We modeled the effect of glacier waters by injecting passive tracers (TRC_GLC) at each of the glaciers′ mouths. After injection, local currents advect the tracers to the northern shelf, whereupon they are ejected into the deep ocean (Figure 8b, Movie S2). The largest tracer concentrations are observed during February and March, following peak discharge. Since TRC_GLC and TRC_SLF have similar ages, their concentrations can be compared. The concentration of TRC_GLC is three orders of magnitude smaller than TRC_SLF, with the difference reflecting the comparative magnitudes of their generating fluxes. At its peak, the flux of TRC_GLC is of the order of 10^3 m^3/s. The flux of TRC_SLF can be roughly estimated by assuming that it is largely concentrated in the northwestern upwelling region. Thus, considering an upwelling area of 50 km in the alongshelf direction and 20 km in the cross-shelf direction and multiplying by a typical upwelling velocity of 10 m/day gives a surface flux of 10^5 m^3/s, which is two orders of magnitude larger than the combined maximum of the glacial discharges. This is, of course, a lower limit to the benthic flux, since obduction of these waters occurs not only in the northwestern region but also across the entire shelf. It is important to note, however, that the larger benthic fluxes do not necessarily imply that iron injection by glacial discharges is negligible, since the amount of bioavailable iron in glacial discharges can be much larger than that of the benthic waters. Evaluation of the quantity of bioavailable iron in glacial discharge and its effect in the ocean is beyond the scope of the present study.
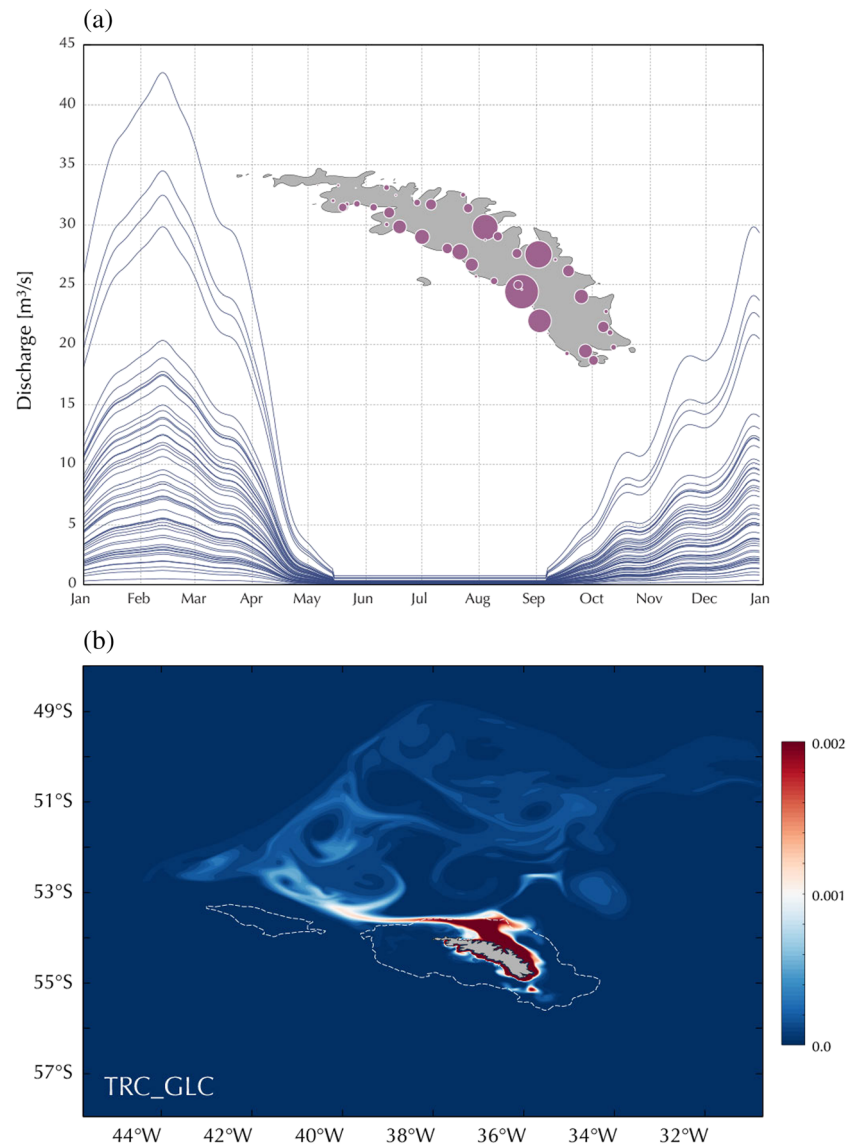
Figure 8. Glacier discharges: (a) time series of glacier discharges implemented in the model. The magenta circles in the inset figure show the location of the discharges. The radius of these circles is proportional to the amplitude of the glacier discharge (after Young et al., 2011), (b) snapshots of the surface tracer distribution of TRC_GLC after a 1 -year diagnostic run. Note that the range of the color bar has changed.

3.6. Seamounts

Meredith (2003) related a chlorophyll patch over the North West Georgia Rise (NWGR), a seamount located to the north of the SG shelf, to the presence of a quasi-permanent anticyclone in this region. There are numerous other seamounts surrounding SG. To assess their potential contribution to the fertilization of shelf and open ocean waters, we released tracers in the bottom layers ($z > 2,000$ m) of two seamounts located to the south of SG and on the NWGR. The plumes generated by these tracers are similar to previous ones (Figure S3). The waters detrained from the seamounts are rapidly advected by the SACCF toward the SG slope and from there onto the bottom layers of the SG shelf, where they are brought to the surface, predominantly on the northwest shelf, by the local wind-driven upwelling. None of the tracer released at the two southern seamounts leads to the development of local (over the seamount) tracer maxima because horizontal velocities in the open ocean are orders of magnitude larger than vertical velocities. The relatively small velocities at the center of the NWGR anticyclone, however, allow the tracer over the top of the seamount
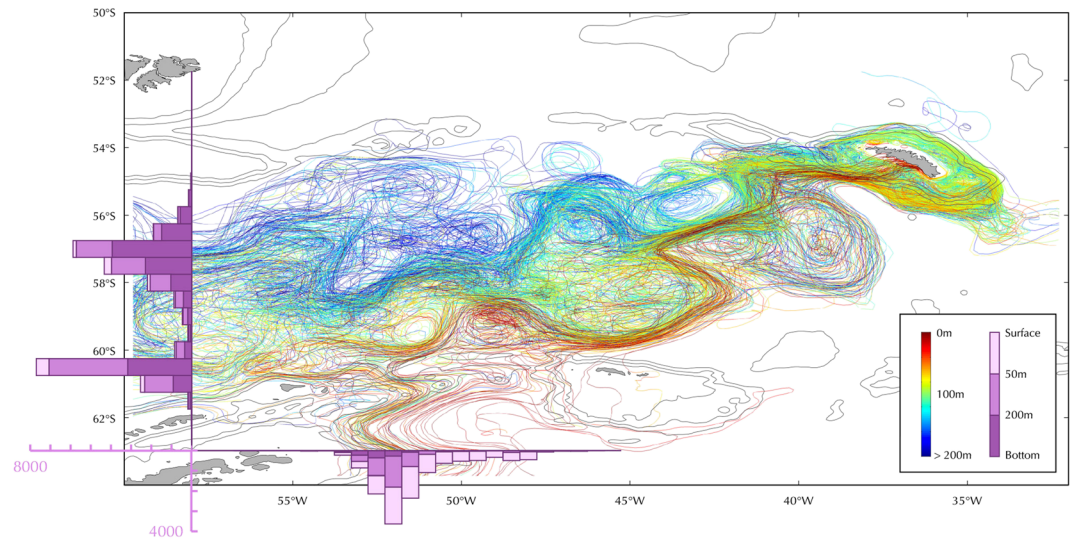
Figure 9. Water mass origins: Trajectories of water parcels toward the SG Island. To generate this plot we seeded 45,085 floats over the SG shelf region and did a backtracking integration using the model's 3-D velocity field to find their origins. Floats were uniformly distributed between 5 and 500 m every 5 m and backtracked during a 720-day period. At the end of the integration, we found that 28,010 floats crossed the cross-section at 58°W (Scotia Sea) and 13,606 from the one at 63°S (Weddell Sea). The remaining 3,469 floats had not still reached those regions. Trajectories color represents the depth of the particles. For clarity, only the trajectories of the particles released at 100 m over the shelf are shown.

to slowly rise toward the surface. This tracer did not reach the surface during our experiment, but it is likely to reach it in longer integrations. Nevertheless, the dominant contribution of this seamount to the obduction process is not through localized upwelling but rather through horizontal advection. NWGR exports most of its tracer-rich waters toward the SG shelf and into the Georgia Basin. The portion of those waters entrained onto the SG shelf is upwelled by the local winds along the northwest coast and by an anticyclone that forms in the southwest portion of the shelf. This anticyclone and the onshore, eddy-driven intrusions of recently upwelled waters, create the peak of tracer concentration in the surface layers of the southwestern sector of SG′s shelf.

3.7. Water Sources

Antarctic krill (*Euphausia superba*) is a vital component of the regional food web and key to supporting colonies of higher predators at SG. The local krill population, however, is not considered to be self-sustaining but is reliant on import from remote sources (Murphy et al., 2007). To identify these sources, Young et al. (2014) implemented a high-resolution model of the SG region and observed that the connection between the shelf and the open ocean was modulated by the proximity and orientation of the SACCF. To identify SG′s water sources, we backtracked the trajectories of 45,085 particles that, in the initial state, were uniformly distributed over the shelf with one particle at every horizontal grid point and from 10 m to the bottom at 10-meter intervals. Particle trajectories were calculated off-line, with the backward-in-time Lagrangian particle-tracking method described in Batchelder (2006). A comprehensive discussion of these types of methods can be found in Van Sebille et al. (2018) and references therein. A census after a 720-day integration identified 28,010 particles originating in the western limit of the Scotia Sea (58°W) and 13,606 in the northwest Weddell Sea (63°S; Figure 9). According to this estimate, approximately two-thirds of SG′s waters were originally located in the Scotia Sea and one-third in the Weddell Sea. Particles from the Scotia Sea originated in deeper layers than those of the Weddell Sea. During their transit toward the shelf, particles undergo intense recirculations and vertical displacements (Figure 9). These migrations are exemplified by the track of a particle originating in the surface layers of the southwestern Scotia Sea (Movie S2). This particle is advected by the SACCF toward the southern coast of SG where it sinks to the bottom and is advected to the northwest coast whereupon it is brought to the surface again by the local wind-driven upwelling. Water parcels following such trajectories will mix with bottom waters during their vertical excursions,
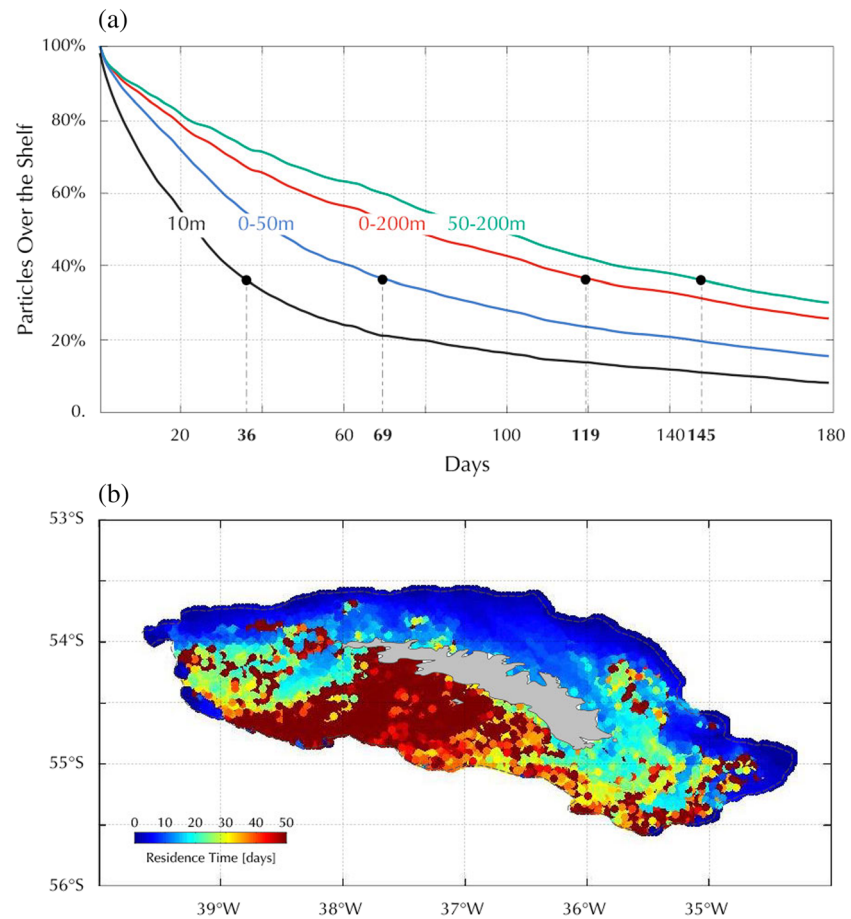
Figure 10. Residence times: This plot shows the time (days) that it takes to floats released over the SG shelf to detrain to the open ocean. We released 225,000 floats/month. At the initial state, these floats were uniformly distributed between 10 m and the bottom at 5-m intervals. Residence time is defined as the time it takes to evacuate 63% of the floats (e-folding time). To evaluate depth-dependence, the floats are divided into four groups: 10 m, 0–50 m, 0–200 m, 50–200 m, with membership dictated by the initial position of the floats: (a) residence time for each float group, (b) regional distribution of residence times for the 11,700 particles released at 10 m on January.

increasing their iron content and further contributing to the surface fertilization of the SG region. Note that this (backward in time) integration does not includes the trajectories of particles that do not reach SG.

3.8. Residence Times

We use particle tracking to estimate the time spent by water parcels over the SG shelf. During the last year of the CTRL experiment, 225,000 particles are released every month. These particles are uniformly distributed between 10 m and the bottom, at 5-m intervals, over the shelf. Residence time is defined as the time taken to evacuate 63% of the particles from the shelf (e-folding time). To evaluate depth-dependence, particle initial positions are divided into four depth groups: 10 m, 0–50 m, 0–200 m, and 50–200 m. We do not include in this estimate the residence times for deeper regions (i.e., 200–500 m), since they only encompass the shelf canyons.

Residence time varies with the initial vertical position of the particles; it is, for example, 69 days for particles released in the upper layer (0–50 m) and approximately double that (145 days) for those released in the deeper layer (50–200 m; in January; Figure 10a). Residence times are not equivalent to advective time, which is the time that it takes a fluid parcel to leave the shelf area when advected by the horizontal velocity field of the release depth. In fact, although the grouping of particles according their initial location is a convenient way to characterize upper and deeper level residence times, particles do not remain in their initial level but move up and down the water column, thus changing the dynamical mechanisms controlling their residence times

Table 1
Numerical Experiments

Name	Initial stratification	Forcing	OBCs
CTRL	HYCOM	Tides, Winds, Sfluxes, and Bfluxes	Seasonal surface and boundary forcing
NWIND_CLI	"	Tides, Sfluxes, and Bfluxes	No winds
NTIDE_CLI	"	Winds, Sfluxes, and Bfluxes	No tides
NW&T_CLI	"	Sfluxes and Bfluxes	No tides or winds
TIDE_BAR	T and S constant	Tides, no Sfluxes, or Bfluxes	Barotropic, no winds
WIND_BAR	"	Winds, no Sfluxes, or Bfluxes	Barotropic, no tides
W&T_BAR	"	Tides + winds, no Sfluxes, or Bfluxes	Barotropic

Note. Characteristics of the numerical experiments described in the text.
Abbreviations: Sfluxes = surface fluxes; Bfluxes = open boundary fluxes.

(e.g., Matano et al., 2019). Residence times not only depend on the initial depth of the fluid parcels but also on their geographical location (Figure 10b). Fluid parcels in the south central and southwestern portions of the shelf have considerably longer residence times than those elsewhere. By contrast, fluid parcels in the northern regions have the shortest residence time. These conclusions are similar to those reported by Young et al. (2014), who observed that the southwestern region has the slowest flushing rates and the northern region the highest.

SG is host to large colonies of higher predators; many of which are constrained to foraging over short distances during breeding, for example, macaroni penguins (Trathan et al., 2006). The rate of flushing has consequences for the replenishment of depleted food reserves, with subsequent impacts on the length and success of predator foraging trips. Macaroni penguin colonies are principally located along the northwestern coast of the mainland close to regions with more rapid flushing and higher rates of replenishment of prey.

4. Circulation Drivers

To characterize the roles of wind, tides, and the open ocean circulation in the SG circulation, we conducted two suites of process-oriented experiments, one barotropic and one baroclinic (Table 1). The barotropic suite, which is initialized with constant values of temperature and salinity, includes three experiments: TIDE_BAR, which is only forced with tides (eight harmonics); WIND_BAR, which is only forced with monthly mean winds, and W&T_BAR, which is forced with the tides and monthly mean winds. Barotropic experiments are run in stand-alone mode using the second-child model and do not include the open ocean circulation. The baroclinic suite is initialized as CTRL, run in the second child model, and forced at the open boundaries with CTRL climatological fields. The baroclinic experiments are NW&T_CLI, which includes wind and tidal forcing, NWIND_CLI, which includes tides but no wind forcing, and NTIDE_CLI, which includes wind but no tidal forcing. All experiments are spun up to dynamical equilibrium and integrated over a 5-year period. The results discussed here are based on the analysis of the last 3 years of each experiment.

4.1. Barotropic Experiments

Experiment TIDE_BAR characterizes the tidally driven portion of the shelf circulation. Tidal amplitudes are relatively small, with peaks of 35 and 18 cm for the two main semidiurnal components (M_2 and S_2) and of ~8 cm for the main diurnal components (K_1 and O_1). Tides from our regional model compare reasonably well with those from the TPXO8 atlas (S4, Egbert et al., 1994), and with the tide gauge values reported by Young et al. (2011). Semidiurnal tidal amplitudes are always larger than diurnal but diurnal harmonics generate the maximum dissipation rates along the shelf break and over the Shag Rocks (S5). Young et al. (2011) posited that this phenomenon is associated with resonance with the diurnal shelf wave. The tidal residual circulation is characterized by an anticyclonic shelf break jet, an intensified coastal current along the northern coast of SG and an anticyclonic vortex over the northeastern seamount (Figure 11a). The net alongshelf and cross-shelf transports generated by the tidal residual currents are relatively small (~0.04 and 0.06 Sv, Table 2). The largest cross-shelf exchanges are observed at the northwestern and southwestern shelf edges.
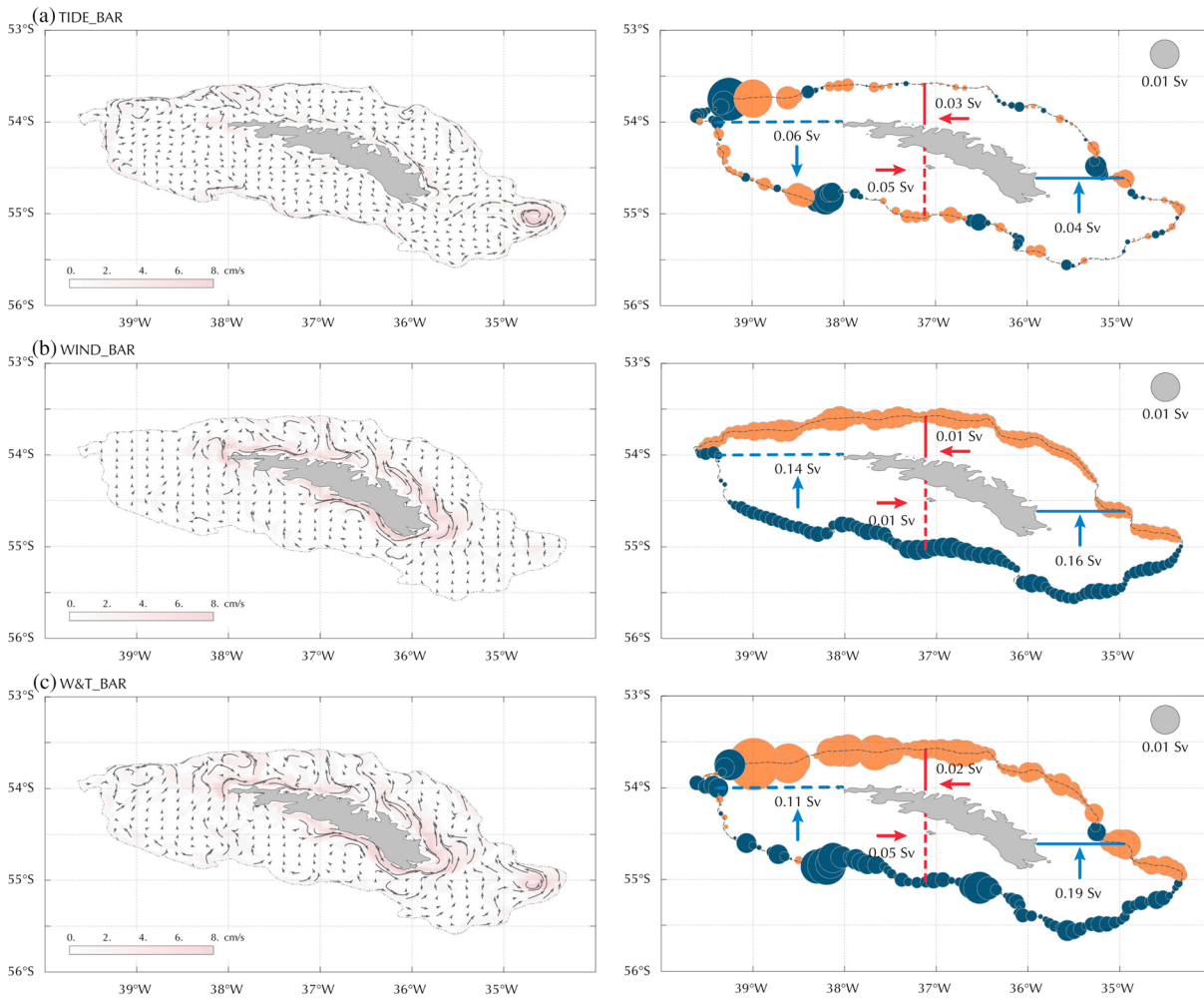
Figure 11. Barotropic experiments: Left panels show the time- and depth-averaged circulation and the right panels cross-shelf (circles) and alongshelf (arrows) transports: (a) TIDE_BAR, (b) WIND_BAR, and (c)T&W_BAR. Background colors in the left panel represent the currents' speeds.

Experiment WIND_BAR characterizes the wind-driven portion of the shelf circulation. Its circulation patterns are consistent with those expected from linear Ekman dynamics, for example, a general northward flow constrained to the uppermost layer (~20 m) over the open portion of the shelf and a geostrophically balanced flow along the coastline (Figure 11b). Circulation patterns near the coast are similar to those of CTRL (Figure 3). Away from the coast, however, the velocity field of WIND_BAR is significantly weaker and lacks the convoluted structure created by the bottom topography. The net cross-shelf mass exchange (0.35 Sv) is one order of magnitude larger than that of TIDE_BAR (Table 2). Cross-shelf exchanges are characterized by an inflow in the southern portion of the shelf and an equivalent outflow in the north. Meridional alongshelf transports are at least three times larger than zonal ones, thus reflecting the small retention of the shelf region on wind-driven inflows.

W&T_BAR combines features of the two previous cases (Figure 11c). Near the coast, the circulation is similar to WIND_BAR, while away from the coast, it is more similar to TIDE_BAR. Comparison with CTRL show obvious similarities (cf. Figures 3 and 11c), most

Table 2
Sensitivity Experiments

Stratification	Name	Along trans.	Cross trans.
Barotropic	WIND_BAR	0.03	0.35
"	TIDE_BAR	0.04	0.06
"	T&W_BAR	0.04	0.38
Baroclinic	**CTRL**	**0.28**	**0.70**
"	NWIND_CLI	0.35	0.53
"	NTIDE_CLI	0.18	0.69
"	NW&T_CLI	0.19	0.48

Note. Mean alongshelf and maximum cross-shelf transports in all the experiments discussed in this article. Mean alongshelf transports are estimated between the coast and the 500 m isobath (e.g., mean value of the curve plotted in Figure 5a). Maximum cross-shelf transport is estimated as the amplitude of alongshelf transport variations (e.g., amplitude of Figure 5a). Values are given in Sverdrups (1 Sv = 10^6 m^3/s).
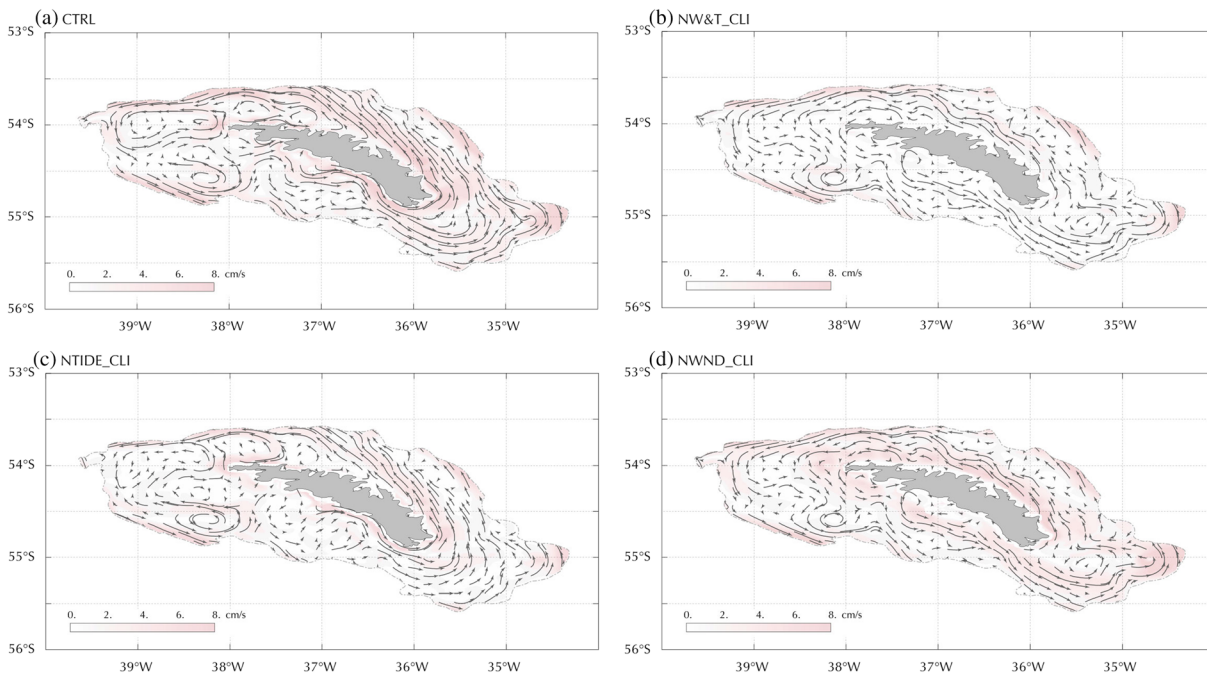
Figure 12. Baroclinic experiments: Time- and depth-averaged circulation in the four baroclinic experiments: (a) CTRL, (b) NW&T_CLI, (c) NTIDE_CLI, and (d) NWND_CLI. Background colors show the currents' speeds.

notably in the coastal circulation jets, anticyclonic vortices near the eastern and western ends of the shelf and weaker flows in the region to the south of the island. CTRL circulation patterns, however, are smoothed by the density stratification. The largest differences between W&T_BAR and CTRL are in the outer shelf region, where the influence of the open ocean circulation is most strongly felt. Shelf/open-ocean exchanges in CTRL are twice as large as in W&T_BAR (Table 2).

4.2. Baroclinic Experiments

These experiments consider the impact of density stratification and open-ocean circulation on the shelf circulation. The first member of this suite is NW&T_CLI, which lacks local tidal and wind forcing, leaving the open ocean circulation as the only driver. Comparison with CTRL shows a significantly weakened circulation pattern, particularly in the middle and inner portions of the southern shelf (Figures 12a and 12b). Open-ocean intrusions are largely funneled to the northeastern region, where they lead to the formation of a westward-flowing jet that resembles that of CTRL. Addition of local wind stress forcing (experiment NTIDE_CLI) increases the similarity with CTRL. Most importantly, it leads to stronger flows near the coastline, particularly in the northwestern region, which now includes the upwelling jet (Figure 12c). The circulation patterns of NTIDE_CLI, however, are still visibly weaker than those of CTRL. The last experiment of this suite, NWIND_CLI, includes tidal but not (local) wind forcing. Tides have two opposing effects on circulation: They enhance the bottom friction, which weakens the circulation, but they also generate rectified flows that enhance it. Comparison of NW&T_CLI and NWND_CLI shows that the latter effect is dominant (Figures 12b and 12d). Tides enhance bottom-trapped vortices, the eastward current flowing along the southern coast and the northwestern jet, leading to the development of a broad anticyclonic shelf flow (Figure 12d). In CTRL, this flow is disrupted by the wind-driven upwelling jet, which diverts a substantial portion offshore (Figure 12a). Note that TIDE_BAR shows an anticyclonic flow similar to that of NWIND_CLI albeit less intense (Figure 11a).

To quantify the contribution of the different drivers to the shelf/open ocean exchanges, we computed along- and cross-shelf transports (Figure 13, Table 2). The curves of the barotropic experiments WIND_BAR and T&W_BAR show positive slopes in the southern portion of the shelf (Pt0 to Pt300) and negative slopes in the northern portion (Pt300 to Pt600), which represent mass inflows in the south and mass outflows in the north. Experiment TIDE_BAR has a constant alongshelf transport and no significant cross-shelf
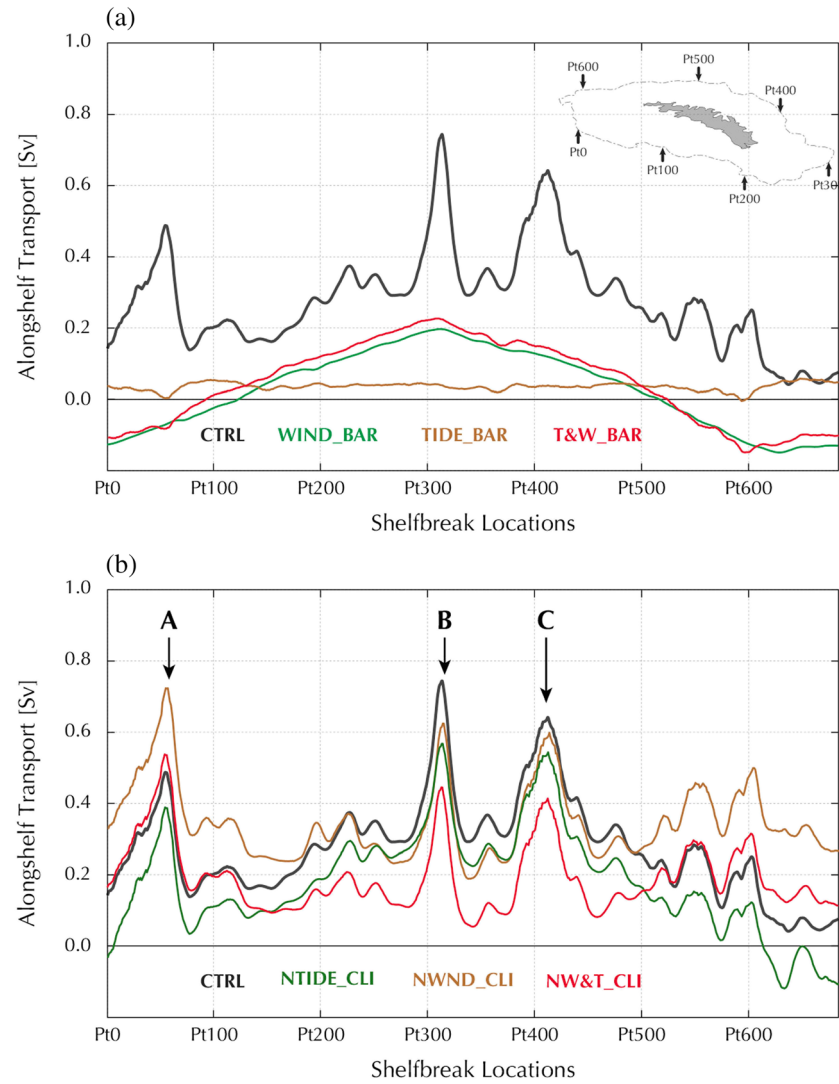
Figure 13. Cross-shelf exchanges: Alongshelf transports in the suite of (a) barotropic and (b) baroclinic process-oriented experiments. The slope of each of these curves is proportional to the cross-shelf transports at each respective location. The location of each of the ordinate points is shown in the inset of panel (a).

transport (Figure 13a, Table 2). CTRL net alongshelf and cross-shelf transports are 0.28 Sv and 0.70 Sv (Table 2); only experiment NTIDE_CLI has a comparable cross-shelf transport (0.69), thus highlighting the retention properties of the circulation arising from tidal forcing. Tidal forcing also enhances the alongshelf circulation; experiment NWIND_CLI has the largest alongshelf transport (0.35 Sv) of the baroclinic suite (Table 2). The alongshelf transport curves of the baroclinic experiments show peaks at identical geographic locations. As noted above, these peaks represent regions where the SACCF impinges on the shelf. There, entrainments and detrainments are nearly compensating so that the net cross-shelf exchange is relatively small. Aside from local peaks, the broad slopes of experiment CTRL are qualitatively similar to those of NTIDE_CLI, thus illustrating the influence of wind forcing on the cross-shelf exchanges. Indeed, it should be noted that if the regional maxima are eliminated, the slopes of CTRL are nearly identical to those of T&W_BAR, which is the barotropic experiment that is only forced by wind and tides. Our analysis, therefore, suggests that wind forcing is the main driver of the shelf/open-ocean exchange. This conclusion, of course, only applies to the long-term average since eddies and meanders can generate episodes of large shelf/open-ocean exchange.

5. Summary

The ocean dynamics driving the fertilization of the waters around SG involve shelf and open ocean obduction and highly energetic interactions between these regions. The SG shelf circulation, which is dominated by a broad anticyclonic gyre superimposed on small vortices, promotes the obduction of deep and benthic waters drawn from the shelf as well as from the open ocean. These waters are then transported toward the Georgia Basin where the steering effect of the bottom topography allows their retention for longer than would be expected elsewhere in the ACC domain. SG's waters are also fertilized by glacial discharges. Lack of iron content data prevents the ranking of the glacier discharge contributions directly; however, a coarse estimate suggests that glacial fluxes are orders of magnitude smaller than other sources.

A suite of process-oriented experiments shows that the SG shelf circulation patterns are driven by winds, tides, and shelf/open-ocean interactions. Tides and wind forcing play distinct roles in the SG circulation. Tides do not contribute significantly to the cross-shelf exchanges, but they strengthen significantly the alongshelf transport. Wind forcing has a negligible impact on the alongshelf transport, but it is the main driver of cross-shelf exchanges. Wind forcing also generates important upwelling in the northwestern portion of the island. Although tides and winds play dominant roles in the steering of the shelf circulation and the shelf/open-ocean exchanges, the ultimate driver of SG productivity is the SACCF, which supplies the deep, iron enriched waters that sustain the development of its exceptional chlorophyll blooms. In a forthcoming article, we will describe the dynamical processes responsible for the obduction of these waters and their sensitivity to climate change.

Data Availability Statement

The ROMS/AGRIF model used in this study can be downloaded from https://www.croco-ocean.org/download/roms_agrif-project/. HYCOM model data can be obtained from https://www.hycom.org. ERA-Interim global atmospheric reanalysis data can be downloaded from https://apps.ecmwf.int/datasets/data/interim-full-daily/levtype=sfc. COADS data can be downloaded from https://iridl.ldeo.columbia.edu/SOURCES/. COADS. Bottom topography data can be obtained from https://www.gebco.net/.

References

Atkinson, A. (2001). South Georgia, Antarctica: A productive, cold water, pelagic ecosystem. *Marine Ecology Research Series*, *216*, 279–308. https://doi.org/10.3354/meps216279

Batchelder, H. P. (2006). Forward-in-time-/backward-in-time-trajectory (FITT/BITT) modeling of particles and organisms in the coastal ocean. *Journal of Atmospheric and Oceanic Technology*, *23*(5), 727–741. https://doi.org/10.1175/JTECH1874.1

Borrione, I., Aumont, O., Nielsdóttir, M. C., & Schlitzer, R. (2014). Sedimentary and atmospheric sources of iron around South Georgia, Southern Ocean: A modelling perspective. *Biogeosciences*, *11*(7), 1981–2001. https://doi.org/10.5194/bg-11-1981-2014

Brandon, M. A., Murphy, E. J., Whitehouse, M. J., Trathan, P. N., Murray, A. W. A., Bone, D. G., & Priddle, J. (1999). The shelfbreak front to the east of the sub-Antarctic Island of South Georgia. *Continental Shelf Research*, *19*(6), 799–819. https://doi.org/10.1016/S0278-4343(98)00112-5

Clowes, A. J. (1938). Phosphate and silica in the Southern Ocean. *Discovery Report*, *19*, 1–120.

Combes, V., & Matano, R. P. (2014). A two-way nested simulation of the oceanic circulation in the Southwestern Atlantic. *Journal of Geophysical Research: Oceans*, *119*, 731–756. https://doi.org/10.1002/2013JC009498

Combes, V., & Matano, R. P. (2019). On the origins of the low-frequency sea surface height variability of the Patagonia shelf region. *Ocean Modelling*, *142*, 101454. https://doi.org/10.1016/j.ocemod.2019.101454

Da Silva, A. M., Young, C. C., & Levitus, S. (1994). Atlas of surface marine data 1994, Vol. 1, algorithms and procedures. *NOAA Atlas NESDIS 6* (pp. 1–74). USA: U.S. Department of Commerce, NOAA, NESDIS.

de Baar, H. J., de Jong, J. T., Bakker, D. C., Löscher, B. M., Veth, C., Bathmann, U., & Smetacek, V. (1995). Importance of iron for plankton blooms and carbon dioxide drawdown in the Southern Ocean. *Nature*, *373*(6513), 412–415. https://doi.org/10.1038/373412a0

Deacon, G. E. R. (1933). A general account of the hydrography of the South Atlantic Ocean. *Discovery Report*, *7*, 171–238.

Debreu, L., Marchesiello, P., Penven, P., & Cambon, G. (2011). Two-way nesting in split-explicit ocean models: Algorithms, implementation and validation. *Ocean Modelling*, *49*, 1–21.

Dee, D. P., Uppala, S. M., Simmons, A. J., Berrisford, P., Poli, P., Kobayashi, S., et al. (2011). The ERA-Interim reanalysis: Configuration and performance of the data assimilation system. *Quarterly Journal of the Royal Meteorological Society*, *137*(656), 553–597. https://doi.org/10.1002/qj.828

Egbert, G. D., Bennett, A. F., & Foreman, M. G. G. (1994). TOPEX/POSEIDON tides estimated using a global inverse model. *Journal of Geophysical Research*, *99*(C12), 24,821–24,852. https://doi.org/10.1029/94JC01894

Fach, B. A., & Klinck, J. M. (2006). Transport of Antarctic krill (*Euphausia superba*) across the Scotia Sea. Part I: Circulation and particle tracking simulations. *Deep-Sea Research Part I: Oceanographic Research Papers*, *53*, 987–1010.

Hardy, A. C., & Gunther, E. R. (1935). The plankton of the South Georgia whaling grounds and adjacent waters, 1926-27. *Discovery Report*, *11*, 1–456.

Harmer, S. F. (1931). Southern whaling. *Proceedings of the Linnean Society of London*, *142*, 85–163.

Hart, T. J. (1934). The plankton of the southwest Atlantic and the Bellingshausen Sea 1929–1931. *Discovery Report*, *8*, 1–268.

Heywood, K. J., Barton, E. D., & Simpson, J. H. (1990). The effects of flow disturbance by an oceanic island. *Journal of Marine Research*, *48*(1), 55–73. https://doi.org/10.1357/002224090784984623

Holeton, C. L., Nédélec, F., Sanders, R., Brown, L., Moore, C. M., Stevens, D. P., et al. (2005). Physiological state of phytoplankton communities in the Southwest Atlantic sector of the Southern Ocean, as measured by fast repetition rate fluorometry. *Polar Biology*, *29*(1), 44–52. https://doi.org/10.1007/s00300-005-0028-y

Korb, R. E., & Whitehouse, M. (2004). Contrasting primary production regimes around South Georgia, Southern Ocean: Large blooms versus high nutrient, low chlorophyll waters. *Deep Sea Research Part I: Oceanographic Research Papers*, *51*(5), 721–738.

Large, W., McWilliams, J., & Doney, S. (1994). Oceanic vertical mixing—A review and a model with a nonlocal boundary-layer parameterization. *Reviews of Geophysics*, *32*(4), 363–403. https://doi.org/10.1029/94RG01872

Marchesiello, P., Debreu, L., & Couvelard, X. (2009). Spurious diapycnal mixing in terrain-following coordinate models: The problem and a solution. *Ocean Modelling*, *26*(3-4), 156–169. https://doi.org/10.1016/j.ocemod.2008.09.004

Matano, R. P., Gordon, A. L., Muench, R. D., & Palma, E. D. (2002). A numerical study of the circulation in the northwestern Weddell Sea. *Deep Sea Research Part II: Topical Studies in Oceanography*, *49*, 4827–4841.

Matano, R. P., Palma, E. D., & Combes, V. (2019). The Burdwood Bank circulation. *Journal of Geophysical Research: Oceans*, *124*, 6904–6926. https://doi.org/10.1029/2019JC015001

Meredith, M. P. (2003). An anticyclonic circulation above the Northwest Georgia Rise, Southern Ocean. *Geophysical Research Letters*, *30*(20), 2061. https://doi.org/10.1029/2003GL018039

Meredith, M. P., Murphy, E. J., Brandon, M. A., Trathan, P. N., Thorpe, S. E., Bone, D. G., et al. (2005). Variability of hydrographic conditions to the east and northwest of South Georgia, 1996-2001. *Journal of Marine Systems*, *53*(1–4), 143–167. https://doi.org/10.1016/j.jmarsys.2004.05.005

Murphy, E. J., Watkins, J. L., Trathan, P. N., Reid, K., Meredith, M. P., Thorpe, S. E., et al. (2007). Spatial and temporal operation of the Scotia Sea ecosystem: A review of large-scale links in a krill centred food web. *Philosophical Transactions of the Royal Society, B: Biological Sciences*, *362*(1477), 113–148. https://doi.org/10.1098/rstb.2006.1957

Orsi, A. H., Whitworth, T. III, & Nowlin, W. D. Jr. (1995). On the meridional extent and fronts of the Antarctic circumpolar current. *Deep Sea Research Part I: Oceanographic Research Papers*, *42*(5), 641–673. https://doi.org/10.1016/0967-0637(95)00021-W

Palacios, D. M. (2002). Factors influencing the island-mass effect of the Galápagos Archipelago. *Geophysical Research Letters*, *29*(23), 2134. https://doi.org/10.1029/2002GL016232

Robinson, J. O. S. I. E., Popova, E. E., Srokosz, M. A., & Yool, A. (2016). A tale of three islands: Downstream natural iron fertilization in the Southern Ocean. *Journal of Geophysical Research: Oceans*, *121*, 3350–3371. https://doi.org/10.1002/2015JC011319

Schlitzer, R. (2002). Carbon export fluxes in the Southern Ocean: Results from inverse modeling and comparison with satellite-based estimates. *Deep Sea Research Part II: Topical Studies in Oceanography*, *49*, 1623–1644.

Shchepetkin, A., & McWilliams, J. C. (2005). The regional oceanic modeling system (ROMS): A split explicit, free-surface, topography-following-coordinate oceanic model. *Ocean Modelling*, *9*(4), 347–404. https://doi.org/10.1016/j.ocemod.2004.08.002

Signorini, S., McClain, C. R., & Dandonneau, Y. (1999). Mixing and phytoplankton bloom in the wake of the Marquesas Islands. *Geophysical Research Letters*, *26*(20), 3121–3124. https://doi.org/10.1029/1999GL010470

Thorpe, S. E., Heywood, K. J., Brandon, M. A., & Stevens, D. P. (2002). Variability of the southern Antarctic circumpolar current front north of South Georgia. *Journal of Marine Systems*, *37*(1–3), 87–105. https://doi.org/10.1016/S0924-7963(02)00197-5

Trathan, P. N., Brierley, A. S., Brandon, M. A., Bone, D. G., Goss, C., Grant, S. A., et al. (2003). Oceanographic variability and changes in Antarctic krill (*Euphausia superba*) abundance at South Georgia. *Fisheries Oceanography*, *12*(6), 569–583. https://doi.org/10.1046/j.1365-2419.2003.00268.x

Trathan, P. N., Green, C., Tanton, J., Peat, H., Poncet, J., & Morton, A. (2006). Foraging dynamics of macaroni penguins *Eudyptes chrysolophus* at South Georgia during brood-guard. *Marine Ecology Progress Series*, *323*, 239–251. https://doi.org/10.3354/meps323239

Van Sebille, E., Griffies, S. M., Abernathey, R., Adams, T. P., Berloff, P., Biastoch, A., et al. (2018). Lagrangian ocean analysis: Fundamentals and practices. *Ocean Modelling*, *121*, 49–75. https://doi.org/10.1016/j.ocemod.2017.11.008

Venables, H. J., & Meredith, M. P. (2009). Theory and observations of Ekman flux in the chlorophyll distribution downstream of South Georgia. *Geophysical Research Letters*, *36*, L23610. https://doi.org/10.1029/2009GL041371

Ward, P., Whitehouse, M., Shreeve, R., Thorpe, S., Atkinson, A., Korb, R., et al. (2007). Plankton community structure south and west of South Georgia (Southern Ocean): Links with production and physical forcing. *Deep Sea Research Part I: Oceanographic Research Papers*, *54*(11), 1871–1889. https://doi.org/10.1016/j.dsr.2007.08.008

Whitehouse, M. J., Korb, R. E., Atkinson, A., Thorpe, S. E., & Gordon, M. (2008). Formation, transport and decay of an intense phytoplankton bloom within high-nutrient low-chlorophyll belt of the southern ocean. *Journal of Marine Systems*, *70*(1-2), 150–167. https://doi.org/10.1016/j.jmarsys.2007.05.003

Whitehouse, M. J., Priddle, J., Brandon, M. A., & Swanson, C. (1999). A comparison of chlorophyll/nutrient dynamics at two survey sites near South Georgia, and the potential role of plankton nitrogen recycled by land-based predators. *Limnology and Oceanography*, *44*(6), 1498–1508. https://doi.org/10.4319/lo.1999.44.6.1498

Whitehouse, M. J., Priddle, J., & Symon, C. (1996). Seasonal and annual change in seawater temperature, salinity, nutrient and chlorophyll a distributions around South Georgia, South Atlantic. *Deep Sea Research, Part I*, *43*, 525–443.

Young, E. F., Meredith, M. P., Murphy, E. J., & Carvalho, G. R. (2011). High-resolution modeling of the shelf and open ocean adjacent to South Georgia, Southern Ocean. *Deep Sea Research Part II: Topical Studies in Oceanography*, *58*(13–16), 1540–1552. https://doi.org/10.1016/j.dsr2.2009.11.003

Young, E. F., Thorpe, S. E., Banglawala, N., & Murphy, E. J. (2014). Variability in transport pathways on and around the South Georgia shelf, Southern Ocean: Implications for recruitment and retention. *Journal of Geophysical Research: Oceans*, *119*, 241–252. https://doi.org/10.1002/2013JC009348